Journal of Astronomical Telescopes, Instruments, and Systems

AstronomicalTelescopes.SPIEDigitalLibrary.org

Analysis of polarization introduced due to the telescope optics of the Thirty Meter Telescope

Ramya Manjunath Anche
Asoke Kumar Sen
Gadiyara Chakrapani Anupama
Kasiviswanathan Sankarasubramanian
Warren Skidmore

SPIE.

Ramya Manjunath Anche, Asoke Kumar Sen, Gadiyara Chakrapani Anupama, Kasiviswanathan Sankarasubramanian, Warren Skidmore, "Analysis of polarization introduced due to the telescope optics of the Thirty Meter Telescope," *J. Astron. Telesc. Instrum. Syst.* **4**(1), 018003 (2018), doi: 10.1117/1.JATIS.4.1.018003.

Analysis of polarization introduced due to the telescope optics of the Thirty Meter Telescope

Ramya Manjunath Anche,[a,*] Asoke Kumar Sen,[b] Gadiyara Chakrapani Anupama,[a] Kasiviswanathan Sankarasubramanian,[a,c] and Warren Skidmore[d]
[a]Indian Institute of Astrophysics, Bangalore, India
[b]Assam University, Department of Physics, Silchar, Assam, India
[c]ISRO Satellite Center, Bangalore, India
[d]Thirty Meter Telescope Corporation, Pasadena, California, United States

Abstract. An analytical model has been developed to estimate the polarization effects, such as instrumental polarization (IP), crosstalk (CT), and depolarization, due to the optics of the Thirty Meter Telescope. These are estimated for the unvignetted field-of-view and the wavelengths of interest. The model estimates an IP of 1.26% and a CT of 44% at the Nasmyth focus of the telescope at the wavelength of 0.6 μm at field angle zero with the telescope pointing to zenith. Mueller matrices have been estimated for the primary, secondary, and Nasmyth mirrors. It is found that some of the Mueller matrix elements of the primary and secondary mirrors show a fourfold azimuthal antisymmetry, which indicates that the polarization at the Cassegrain focus is negligible. At the inclined Nasmyth mirror, there is no azimuthal antisymmetry in the matrix elements, and this results in nonzero values for IP and CT, which would negatively impact the polarization measurements at the telescope focus. The averaged Mueller matrix is estimated at the Nasmyth focus at different instrument ports and various zenith angles of the telescope. The variation in the Mueller matrix elements for different coatings is also estimated. The impact of this polarization effect on the science case requirements has been discussed. This analysis will help in achieving precise requirements for future instruments with polarimetric capability. [DOI: 10.1117/1.JATIS.4.1.018003]

Keywords: instrumental polarization; crosstalk; ray tracing; analytical method; Mueller matrix; Thirty Meter Telescope.

Paper 17025P received Jun. 10, 2017; accepted for publication Dec. 18, 2017; published online Jan. 22, 2018.

1 Introduction

Polarization measurements of celestial sources reveal useful information regarding their magnetic field, scattered dust, stellar, and planetary atmosphere.[1] These measurements are taken using a polarimeter placed at the telescope focus. Ideally, the telescope and instrument optics should not alter or introduce any polarization to the incoming light. However, as shown by the earlier work of Mcguire and Chipman[2] and Stenflo,[3] the instrumental polarization (IP) and polarization aberrations are introduced by lenses and mirrors in the telescope and instruments. It is also seen that the high angle of incidence of the incoming polarized light affects the image quality.[4,5] In addition to this, the telescope optics also cause depolarization (DP) and crosstalk (CT).[6] If the polarization measured at the telescope focus is nonzero for an unpolarized incoming light, then it is termed as IP.[7] DP is the loss of polarization due to the telescope optics when a 100% linearly polarized light is incident and is measured as (100–P)%, where P is the polarization measured at the focus. Additionally, if the telescope system converts the incoming linear polarization to circular or vice-versa, it is called CT. If the optical system has an inherent cylindrical (or azimuthal) symmetry and the object is on the optical axis of the telescope, the polarization introduced by the optics will be canceled out mutually, resulting in zero IP and CT.[7] In general, a Cassegrain system (with the object on the axis of the telescope) is preferred for polarization observations, as it is expected to be free of IP.[1,8] However, in the real scenario, there are several factors that alter the polarization of the incoming light, such as inhomogeneities in the thickness, composition, oxidation, and aging of the coating.[9,10] These are different from the polarization effects caused by the reflection geometries of the telescope and are treated mostly as noise in the measurement. In this work, we describe the polarization effects due to the reflection geometries of the telescope optics with special emphasis on the Nasmyth focus. We have assumed all other conditions to be ideal for our case.

The next generation large telescopes[11,12] consist of a Nasmyth platform on which the instruments are placed. In these systems, the light is directed toward various instruments using a fold mirror (Nasmyth mirror), which is placed after the secondary mirror. It is found that an aluminum-coated fold mirror kept at an inclined angle of 45 deg can give an IP of 2.8% and CT of 18% at a wavelength of 0.63 μm.[13] The dependence of IP on the incident angles of the mirror has already been estimated and presented for silver, gold, and aluminum coating.[14] A model has been developed to estimate the IP at the focus of a very large telescope (VLT).[15] They use Stokes/Mueller formalism to estimate the IP for the telescope and the Nasmyth adaptive optics system (NACO) for the K_s band. The model is compared with the standard star observations. An extensive analysis of the IP at the focus of the European Extremely Large Telescope (E-ELT) has been done.[16] They use the polarimetric system code M&m's to estimate the IP due to the optical

*Address all correspondence to: Ramya Manjunath Anche, E-mail: ramyam@iiap.res.in

2329-4124/2018/$25.00 © 2018 SPIE

path of the E-ELT for a wavelength range of 500 to 900 nm and zenith angle of 0 deg to 90 deg.

Another large segmented mirror telescope, the Thirty Meter Telescope (TMT) is proposed to be built on Mauna Kea in Hawaii,[11] which has a folding mirror in its optical configuration. The potential polarimetric science cases that can be carried o ut with the TMT were collected by the TMT polarimetry and time-resolved capabilities working group (PTRWG).[17] For each observing program, the spectral resolution, wavelength range, maximum polarization measurement error, object type, field size, and the planned instrument type for observing were tabulated. The amount of acceptable IP and CT that could be tolerated while conducting the key polarimetric science programs was found to be 1% to 2% and 1% to 20%, respectively, for different wavelength ranges and field angles. These levels were derived based on the expected errors in calibrating the IP and CT.

The optical design of the TMT is a folded Ritchey–Chretien,[18] where the primary mirror is a concave hyperboloid, with 492 hexagonal segments with each segment being about 1.44 m (56.6 in.) across the corners. The segment gap between the segments is 2.5 mm (0.1 in.) wide.[19] The diameter of the secondary mirror is 3.1 m, which converts the light coming from the primary mirror at $f/1$ to $f/15$ beam for the science instruments on the Nasmyth platforms, as shown in Fig. 1.[20] The Nasmyth (tertiary) mirror is a plane mirror (with elliptical cross-section) of 3.5×2.5 m across and located at the center of the primary mirror. The tertiary mirror will be able to switch among the science instruments rapidly and precisely, and track in two axes to keep the beam aligned with the instrument when the telescope changes zenith angle. The rotation axis is coincident with the primary mirror optical axis, and the tilt axis is perpendicular to that axis. The focal ratio of the telescope is $f/15$, and the image is formed at the Nasmyth foci, 20 m from the center of the tertiary mirror. The unvignetted field-of-view of the telescope is 15 arc min and field-of-view with vignetting is 20 arc min.

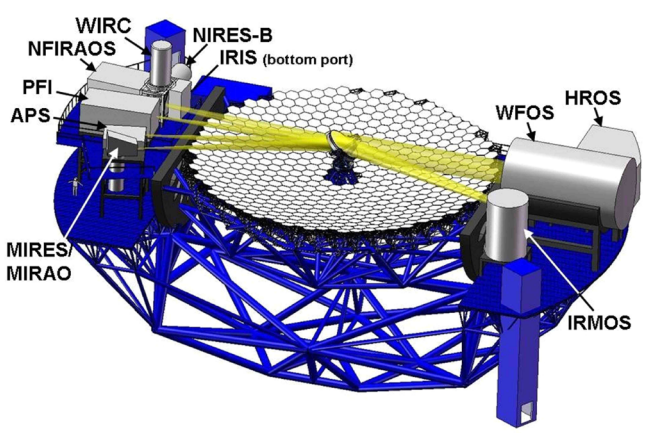

Fig. 1 The Nasmyth platform of the TMT showing the different instrument positions. Wide field optical spectrograph (WFOS) instrument port corresponds to the tilt of 45 deg of the Nasmyth mirror.

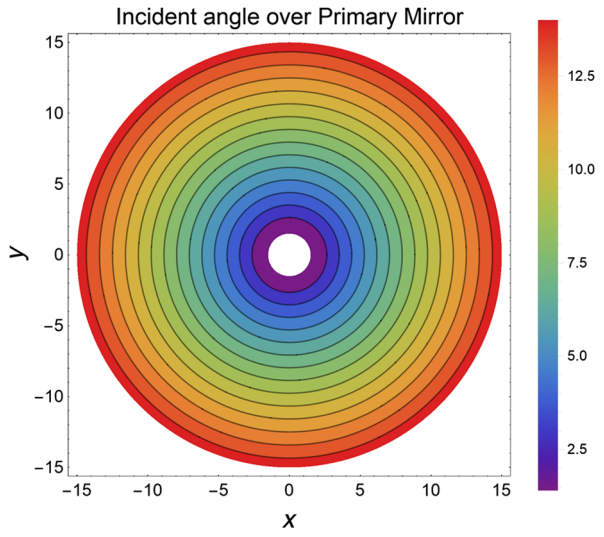

Fig. 2 The incident angles are shown for the on-axis rays on the surface of primary mirror. *x* and *y* are in meters and contour values are given in degrees.

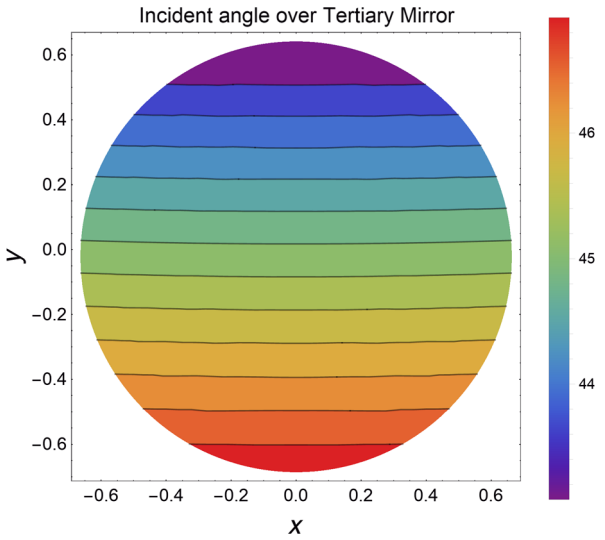

Fig. 3 The incident angles are shown for the on-axis rays on the surface of Nasmyth mirror. *x* and *y* are in meters and contour values are given in degrees.

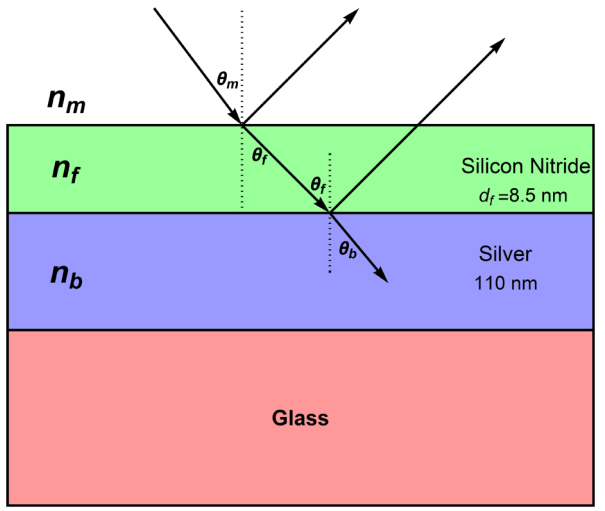

Fig. 4 The coating used in the modeling is shown. Silver is the bulk metal layer. Silicon nitride is the protective layer.

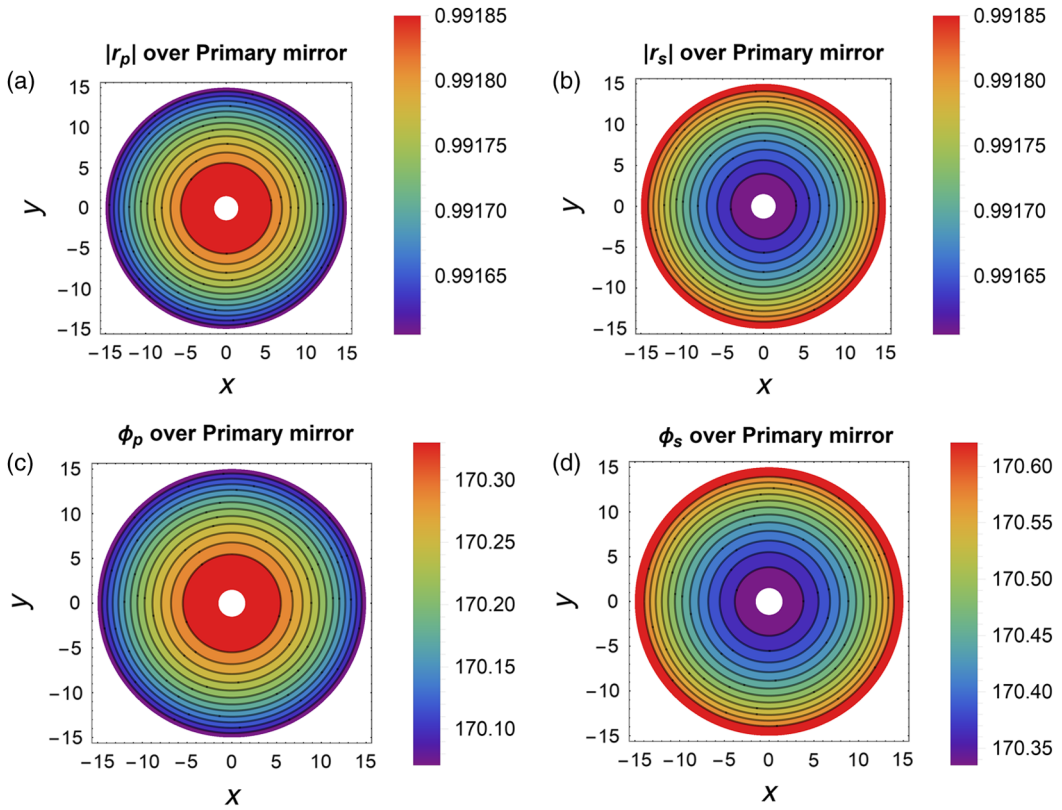

Fig. 5 The reflection coefficients on the mirror surface at $\lambda = 2.583$ μm is shown for the primary mirror. (a) and (b) show the amplitudes and (c) and (d) show the phase of the reflection coefficients. *x* and *y* are in meters. The values for the phases are given in degrees.

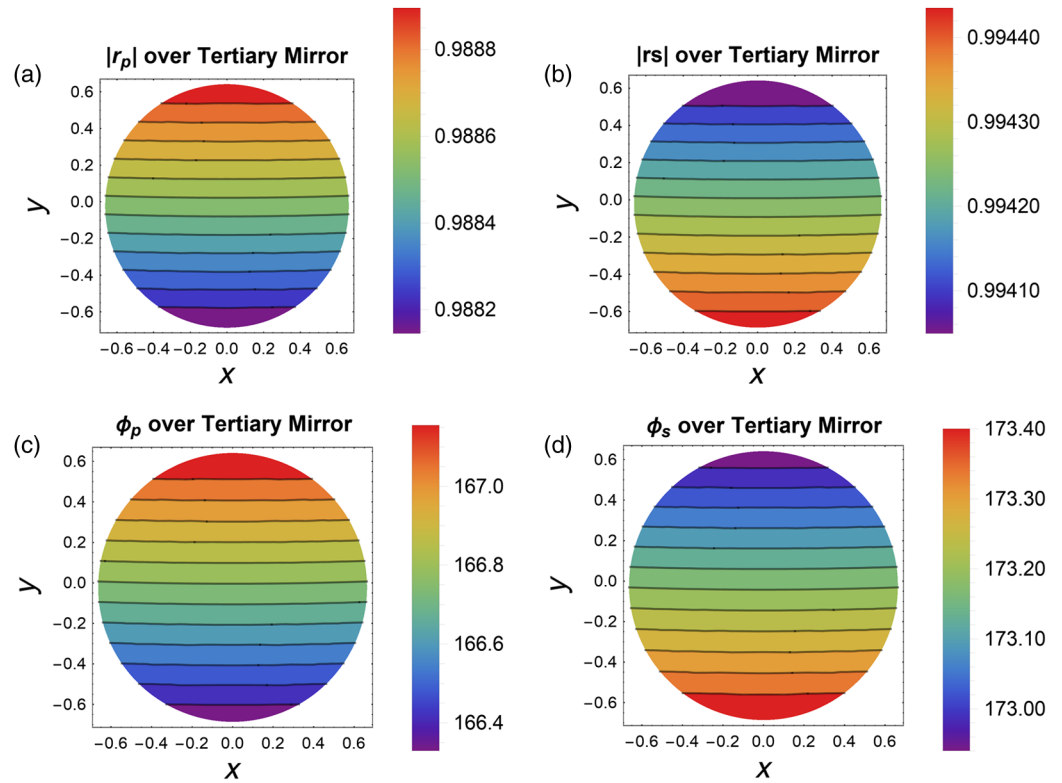

Fig. 6 The reflection coefficients on the mirror surface at $\lambda = 2.583$ μm is shown for the Nasmyth mirror. (a) and (b) show the amplitudes and (c) and (d) show the phase of the reflection coefficients. *x* and *y* are in meters. The values for the phases are given in degrees.

In this paper, we present a complete analysis of the polarization effects due to the optics of the TMT, which is an elaborate and detailed description of the concepts reported earlier in Anche et al.[21] The paper is organized as follows. Section 2 gives the brief summary of the polarization ray tracing algorithm used for the estimation of the polarization effects from the telescope. The algorithm is explained in detail in Appendix A. The variations in the IP, CT, and DP with wavelength ($\lambda = 0.4$ to 2.5 μm) and field angle ($0'$ to $7.5'$) at one of the instrument ports (WFOS) are estimated and presented. Along with this, the contour plots of the Mueller matrix terms explaining the variation of the matrix elements over the mirror surface are presented in Sec. 3. The dependence of Mueller matrix elements on the field angle, instrument position, zenith angle and the mirror coating is shown in Sec. 4. Section 5 discusses the impact of these effects on the science programs and their mitigation, and calibration strategies.

This work would be beneficial in deciding the wavelength range, field-of-view, and the instrument port for any future instrument with polarimetric capability.

2 Polarization Ray Tracing Algorithm

The polarization ray tracing has been described in the past by various authors. In the work by Chipman,[22] the authors have described a polarization ray tracing calculus, which is a generalization of the Jones calculus into three dimensions. They have considered $x - y - z$ coordinate system as the global coordinate system and $p - s$ as the local coordinate system, which is also followed in this paper. In a later work,[23] the IP and DP were calculated at the prime and Cassegrain foci. The polarization ray tracing algorithm (given in Appendix A) for TMT developed in the present work is actually based on the earlier work by Sen and Kakati.[23] It involves tracing of the ray from the primary mirror of the TMT till the Nasmyth focus considering changes in the polarization at each surface. The direction cosine (DC) of the rays is determined at each interface for the incident, reflected rays, and surface normal (which together define a plane). The electric field vector in the rays can be resolved into two orthogonal directions, p-vector, which is parallel to the plane, and s-vector, which is perpendicular to the plane. The DCs of these vectors are also estimated. The Fresnel reflection coefficients[24] r_p and r_s are estimated for the mirror coating. The quantities r_p and r_s represent the amplitude reflection coefficients. These two parameters depend on the location of mirror surfaces from where reflections take place. We use Stokes–Mueller[25] formalism for determining the polarization effects. The Stokes vector for the unpolarized light is [1 0 0 0], which indicates that the amplitude of the electric field vectors in

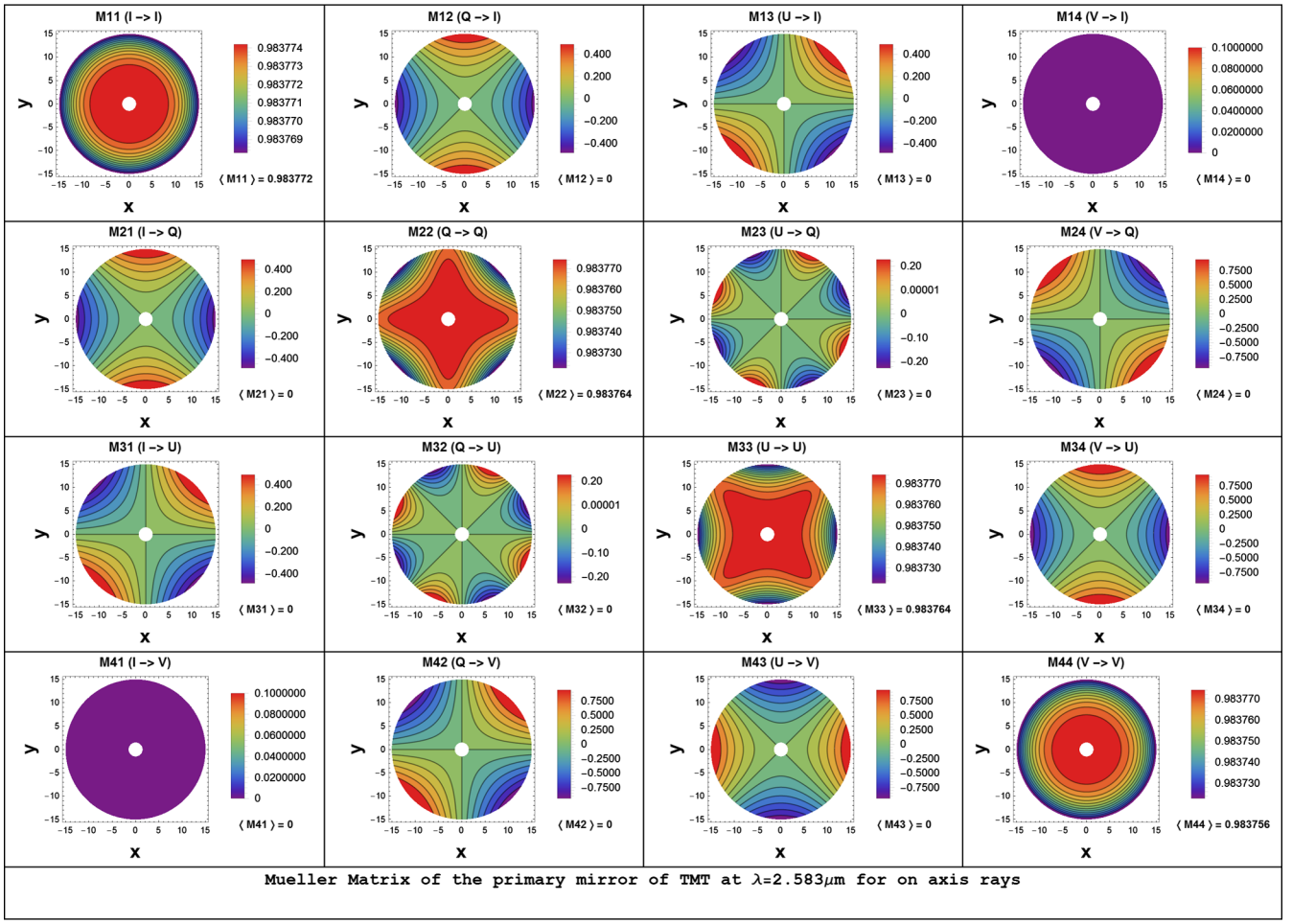

Fig. 7 The Mueller matrix of the primary mirror at a wavelength of 2.580 μm for the on-axis rays. The number of rays is sampled radially. The input Stokes vectors are multiplied with this Mueller matrix to estimate the corresponding output Stokes vectors. The azimuth antisymmetry is seen in all the elements except the diagonal elements, which explains zero IP ($M21$ and $M31$) and CT ($M32$, $M42$, $M43$) for on-axis rays at the prime focus. $\langle\rangle$ gives the average values of the Mueller matrix elements.

$p-s$ frame as $E_p = 1/\sqrt{2}$ and $E_p = 1/\sqrt{2}$.[25] With unpolarized light as input, if the IP is found to be present at the focal plane, then it is indicative of nonzero values of Q, U, and V. For the 100% linearly polarized light with Stokes vectors $[I\ Q\ U\ 0]$, the quantity $\sqrt{Q^2+U^2}$ should be equal to 1. In the present work, we estimate the IP, CT, and DP for such unpolarized and 100% polarized light as inputs for the TMT. To estimate the polarization effects for different input polarization states, the Mueller matrix M can be calculated analytically using reflection coefficients.[13] We have also used the polarization ray tracing algorithm as available in the optical design software Zemax, to compare it with the analytical ray tracing model used in the present work. In Zemax, the polarization pupil map is used to perform polarization ray tracing for a large number of rays for different input polarization states.[17]

3 Polarization Effects at the Telescope Focus

Using the polarization ray tracing algorithm given in Appendix A, incident angles have been estimated on the surface of primary, secondary, and Nasmyth mirrors. The incident angle on primary (shown in Fig. 2) and secondary mirror shows similar variation for the rays parallel to the z-axis. Incident angle varies from 1.43 deg (at the inner edge with a radius of 1.5 m) to 14.0358 deg (at the outer edge of the mirror with a radius 15 m) in the case of the primary. It varies from 1.527 deg to 14.9955 deg for the secondary mirror. The incident angle in the case of the Nasmyth mirror (Fig. 3) increases from 43.0896 deg to 46.9104 deg from one end of the mirror to the other end. One end of the beam (marginal ray) will have a higher angle of incidence compared to the other end, since the converging beam falls on the mirror kept at a tilt of 45 deg.

The mirrors in the TMT telescope will have a four-layer coating,[26] which was initially developed for the Gemini telescope.[27] We are considering Si_3N_x of 85Å and silver of 1100Å for the analysis, as shown in Fig. 4. The refractive index of $NiCrN_x$ (thickness of 65Å and 6Å) was not available in the literature and hence is not considered here.

In Fig. 4, n_b and θ_b are the refractive index and the incident angle at the bulk metal silver layer, respectively, and n_f is the refractive index of Si_3N_4. n_m and θ_m are the refractive index and incident angle for air, respectively. The refractive indices of Si_3N_4 and silver are obtained from Palik.[28] The Fresnel reflection coefficients r_p and r_s for this coating are calculated[9,29] for all three mirrors. We note that r_p and r_s are complex numbers. The contour plots of the reflection coefficients for primary and tertiary are shown in Figs. 5 and 6, respectively. The contours show the same variation as the incident angles show on the mirror surfaces. Figures 5(a) and 5(b) show the amplitude

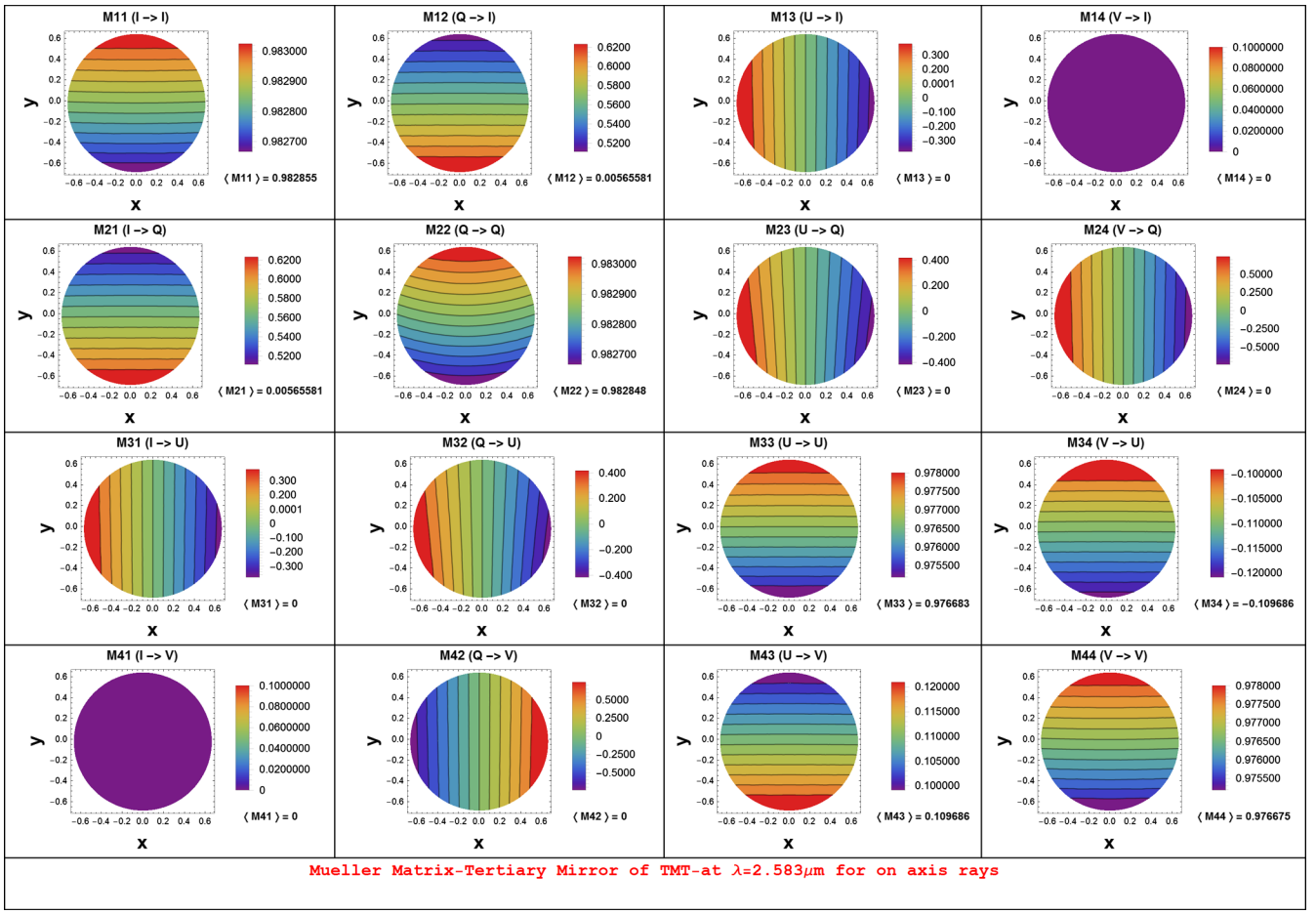

Fig. 8 The Mueller matrix of the Nasmyth mirror at a wavelength of 2.58 μm for the on-axis rays. The contour plots are similar trend as that of the incident angle of the Nasmyth mirror. They show symmetry along one axis of the mirror. IP ($M21$) and CT ($M43$) are found to increase from one end of the mirror to the other. $M31$, $M32$, and $M42$ show equal positive and negative values and gives zero on average. $\langle\rangle$ gives the average values of the Mueller matrix elements.

of r_p and r_s. Figures 5(c) and 5(d) show the corresponding phase components ϕ_p and ϕ_s.

The Mueller matrices are estimated using the reflection coefficients, which show that the polarization effects at prime and Cassegrain focus are zero for the paraxial rays. However, in the case of an off-axis source with field angle 7.5′, the IP is nonzero, with values of 10^{-6} and 10^{-4} at prime and Cassegrain focus, respectively.

The contour plot of the Mueller matrix (M) for the primary mirror is shown in Fig. 7. The $M11$ term in Fig. 7 indicates the intensity values at different regions of the mirror surface. The incident angles are smaller (near normal angle of incidence) at the center of the primary mirror, which indicates that the reflection coefficients are nearly equal. At the periphery, the r_p and r_s values diminish, and hence, the intensity decreases outward. $M11$ is found to vary over the primary mirror surface with wavelength. $M21$ and $M31$ exhibit the division in four quadrants. In the first quadrant 0 deg to 90 deg, the $M21$ on the mirror exhibits positive values and the next quadrant exhibits negative values. When all the rays are added at the focal plane, we get $M21$ and $M31$ as zero at the prime focus for on-axis rays. $M41$ $(I \rightarrow V)$ is found to be zero. These three elements $(I \rightarrow Q, U, V)$ are related to the IP,[13] $M22$ and $M33$ show $Q \rightarrow Q$ and $U \rightarrow U$ which when squared and added, gives I for 100%

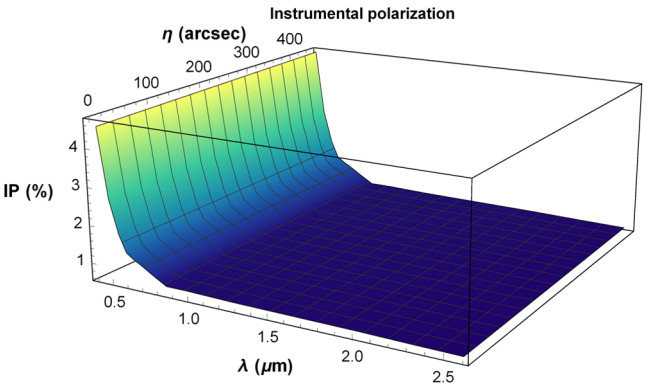

Fig. 9 Variation of IP for semifield of 7.5′ (z-axis) and wavelength range of 0.4 to 2.5 μm (x-axis) is shown at the Nasmyth focus of the TMT. The values are higher near the optical region which is shown by light yellow compared to those in the near infrared region shown by dark blue color.

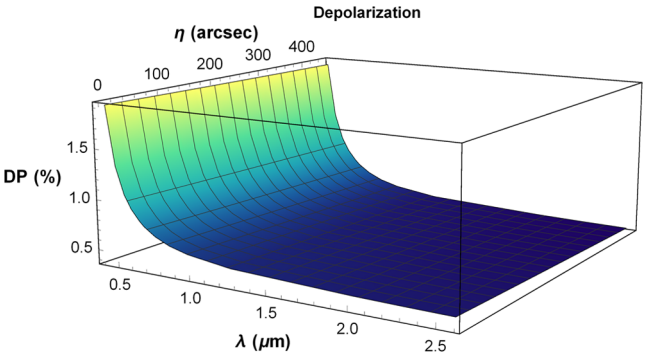

Fig. 10 Variation of DP for semi field of 7.5′ (z-axis) and wavelength range of 0.4 to 2.5 μm (x-axis) is shown in the figure at the Nasmyth focus of TMT. The values are higher near the optical region which is shown by light yellow compared to those in the near infrared region shown by dark blue color.

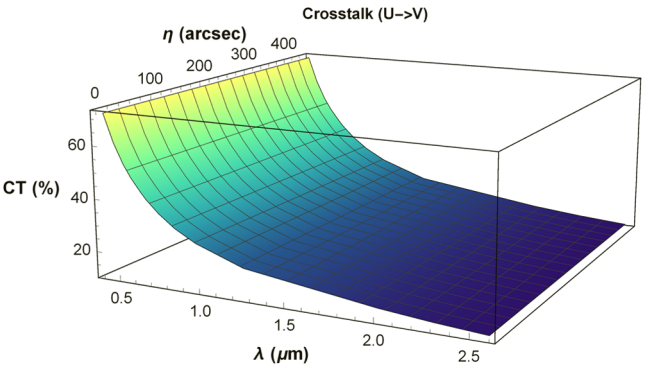

Fig. 11 Variation of CT for semifield of 7.5′ (z-axis) and wavelength range of 0.4 to 2.5 μm (x-axis) is shown in the figure at the Nasmyth focus of TMT. The values are higher near the optical region which is shown by light yellow compared to those in the near infrared region shown by dark blue color.

Table 1 The variation of IP, DP, and CT with wavelength at zero field angle. Here, IP corresponds to the unpolarized light falling on the mirror and DP, CT corresponds to the 100% linearly polarized light falling on the mirror.

Wavelength (μm)	IP (%) $I \rightarrow Q, U$	DP (%)	CT (%) $U \rightarrow V$
0.4	4.54	2.0	72.12
0.4592	2.69	1.35	61.36
0.5166	1.82	1.08	53.64
0.5636	1.37	0.94	48.77
0.6199	1.21	0.83	44.06
0.6526	1.14	0.78	41.54
0.7293	0.94	0.70	36.83
0.8266	0.70	0.64	32.11
0.9537	0.71	0.58	27.66
1.24	0.68	0.52	21.11
2.000	0.65	0.48	14.37
2.296	0.63	0.47	12.53
2.583	0.61	0.46	11.16
Astronomical bands	**IP (%)**	**DP (%)**	**CT (%)**
U, B, V	4.5–1.3	2–1	70–45
R,I	1.2–0.7	1–0.6	45–32
J	0.68	0.53	21
H	0.65	0.48	14
K	0.63	0.47	12
>2.5	<0.6	<0.46	<10

linear polarization as input. $M23$ and $M32$ show that the $U \rightarrow Q$ and $Q \rightarrow U$, respectively. These terms correspond to the polarization rotation. $M42$ and $M43$ correspond to linear to circular polarization CT. Due to antisymmetry, these become zero on average at the focus (which means when polarization states of all the rays are added at the focus). The output Stokes vectors for different polarization states of input ray are obtained by multiplying the input Stokes vectors with this Mueller matrix[25] $[S_{\text{out}}] = M[S_{\text{in}}]$.

The contour plots of the Mueller matrix estimated at the Cassegrain focus display similar behavior as that of the prime focus, as shown in Fig. 7, and are hence not presented here.

The Mueller matrix corresponding to the Nasmyth mirror is shown in Fig. 8. The Mueller matrix elements $M11$, $M22$, $M33$, and $M44$ show a similar trend as that of the incident angle of the Nasmyth mirror. $M12$, $M21$, $M34$, and $M43$ (after reflection from Nasmyth mirror) are same across the major axis of the Nasmyth mirror with a positive contribution from each contour segment. But along the major axis, they are unequal along the two directions. The remaining elements ($M31$, $M32$, $M13$, $M23$, $M24$, and $M42$) have equal positive and negative contributions on either side of the major axis of the ellipse. Hence, a nonzero IP ($M21$) and CT ($M43$) are seen at the Nasmyth focus.

For an unpolarized light falling on the primary mirror, IP was estimated at the Nasmyth focus using the ray tracing algorithm given in Appendix A. It is found to be of the order of 10^{-6} for the primary mirror (for field angle $7.5'$) and of the order of 10^{-4} for the secondary mirror, which are negligible compared with the measurement error (shown in Fig. 18 and 19 in Appendix A respectively). However, for zero field angles, these two values are zero. The plots at the prime and Cassegrain focus have been given in Appendix A for comparison. Figure 9 shows the IP estimated at the Nasmyth focus when the Nasmyth mirror is at $\theta = 0$ deg (rotation) and $\Phi = 45$ (tilt) pointing to WFOS instrument port (Fig. 1). At this instrument port, the tilt of the Nasmyth mirror remains at 45 deg even when the zenith angle of the telescope changes as shown in Eq. (3). In Fig. 9, IP increases linearly with the field angle. It is on the order of 4% to 1.2% in the optical region and 0.6% in the near-infrared region for zero field angle. IP does not change with the zenith angle

$$E = \begin{pmatrix} 1 & 0.453 & 0 & 0 \\ 0.453 & 0.9971 & 0 & 0 \\ 0 & 0 & 0.6766 & 0.7289 \\ 0 & 0 & 0.7308 & -0.6746 \end{pmatrix}. \quad (1)$$

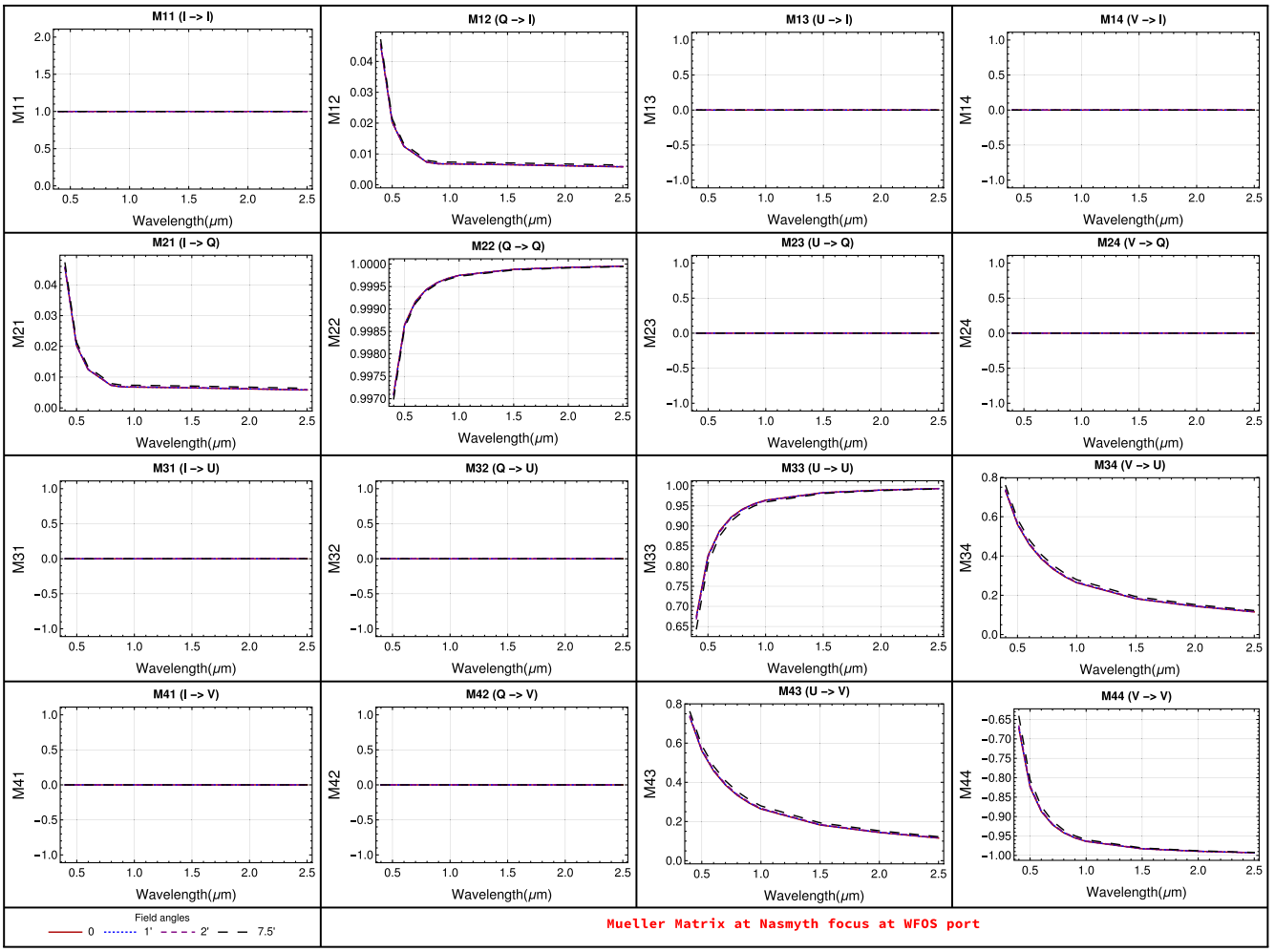

Fig. 12 Normalized Mueller matrices versus wavelength is obtained at the WFOS port of TMT for different field angles. The field angles are indicated by different colors.

The effect of this phenomenon can be seen in a 4×4 Muller matrix as given in matrix 1, which we may call as error matrix (E). The diagonal terms in the matrix 1 are equal to 1 if the optics of the telescope has no effect on the polarization state of the input light and off-diagonal terms are zero. However, our analysis shows that, for an on-axis object, we found there are deviations from these ideal values. Thus, matrix E provides an error estimate during uncalibrated polarization measurement.

In the case of 100% polarized light as the input, the DP has been estimated. It is 0.3% and 1.5% in the case of primary and secondary mirrors, respectively (Figs. 20 and 21 in Appendix A) for the field angle of 7.5′ at 0.4 μm wavelength. In Fig. 10, DP increases with the field angle and is close to 0.8% in the near-infrared region and rises to 2.5% in the optical at the field angle value 7.5′ at the Nasmyth focus at the WFOS instrument port (IBA = 0, IEA = 0). The polarization state of light at the end of the Nasmyth focus has changed to elliptical from 100% linear polarization, which indicates the conversion from U to V. Hence, we estimated the circular polarization at the Nasmyth focus to determine CT (see Fig. 11). CT at the Nasmyth focus increases with the field angle and is found to be higher (70%) in the optical region compared to the near-infrared region (10%), which indicates that circular polarization has to be measured to reconstruct the input linear polarization. The DP and CT do not depend on the pointing of the telescope at this instrument port of TMT. Table 1 shows the IP, DP, and CT at Nasmyth focus for different wavelengths, for rays parallel to the optical axis.

The results of our analysis have been compared with the modeling results of the E-ELT telescope,[16] where an IP of 2% to 3.4% and CT of about 12% to 14% for the wavelength range of 0.5 to 0.9 μm was estimated. The coating used in the polarization modeling of E-ELT is protective aluminum and the optical layout consists of six mirrors,[16] where $M1$, $M2$, and $M3$ are rotationally symmetric. The IP and CT are zenith angle independent for the M4-M5-Nasmyth focus, but zenith angle dependent for M4-M5-M6-Nasmyth focus. In the case of TMT, these values are dependent on zenith angle at all the instrument ports except the instrument port with IBA = 0 and IEA = 0 (WFOS port).[30] In the case of VLT telescope, the estimated IP is 4% for the K_s band for the telescope and the adaptive optics system (NACO).[15]

4 Averaged Mueller Matrices on the Nasmyth Platform

In this section the Mueller matrix is estimated for each ray falling on the primary mirror and averaged at the Nasmyth focus using the polarization pupil map in Zemax.[17] It depends on the reflection coefficients (which vary with the wavelength), and on the incident angle. The incident angles (on the Nasmyth

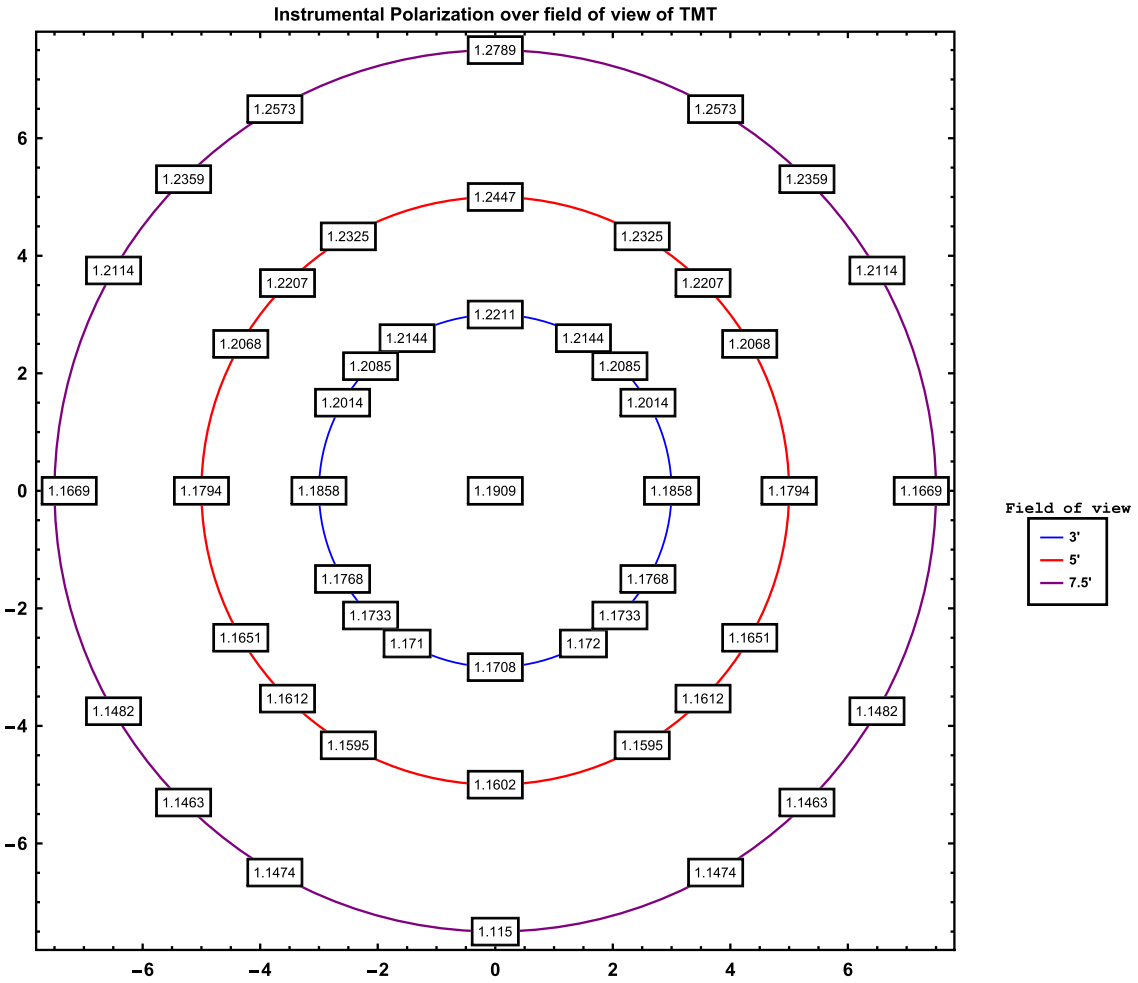

Fig. 13 The IP is estimated at the WFOS port for the field-of-view of the telescope. The three concentric circles represent 3, 5, and 7.5′, respectively. The IP values are written inside the box at each field point.

mirror) vary with the field angle, zenith angle of the telescope and instrument bearing angle (IBA).[30]

4.1 *Mueller Matrices at WFOS Port for Various Field Angles*

The field-of-view of TMT is 15′ without vignetting. The variation of the Mueller matrix elements with different field angles is shown in Fig. 12. The matrix elements do not deviate much with an increase in the field angle. The IP estimated over the field-of-view (on the sky) of the telescope is shown in Fig. 13. The IP values are asymmetric along the major axis of the Nasmyth mirror with the elliptical cross-section. This effect would lead to polarization variation issues in the case of imaging polarimetry of extended sources.

4.2 *Mueller Matrices at Different Instrument Ports of TMT*

As shown in Fig. 1, currently, there are eight instrument ports on the Nasmyth platform for TMT. The first generation instruments are going to be Wide Field Optical Spectrometer (WFOS), Narrow Field Infrared Adaptive Optics System (NFIRAOS) and Infrared Imaging Spectrograph (IRIS) The rotation (θ) and tilt (Φ) for the Nasmyth mirror changes for different instrument ports and zenith angles of the telescope. The coordinate system used to derive these angles is explained in the TMT design requirements document:[30]

$$\theta = \arctan\left(\frac{\cos\,\zeta\,\cos(\mathrm{IEA})\sin(\mathrm{IBA}) - \sin\,\zeta\,\sin(\mathrm{IEA})}{\cos(\mathrm{IEA})\sin(\mathrm{IBA})}\right), \tag{2}$$

$$\Phi = 0.5\,\arccos[-\sin\,\zeta\,\cos(\mathrm{IEA})\sin(\mathrm{IBA}) + \cos\,\zeta\,\sin(\mathrm{IBA})], \tag{3}$$

where ζ corresponds to the zenith angle of the telescope. It varies from 0 deg and 65 deg. IEA is the instrument elevation angle and IBA is the instrument bearing angle. θ and Φ correspond to the rotation and the tilt of the Nasmyth mirror depending on the instrument position. IEA = 0 for all the instrument ports as the focal plane of all the instruments intercepts with the telescope focal plane. With IEA = 0, the tilt and rotation of the mirror depend on IBA and the zenith angle of the telescope. For the $\zeta = 0$, the Mueller matrix at different instrument ports can be obtained by $M_{\mathrm{inst}} = M_{\mathrm{WFOS}}R(\theta)$, where θ corresponds to the rotation of the tertiary mirror from its initial position

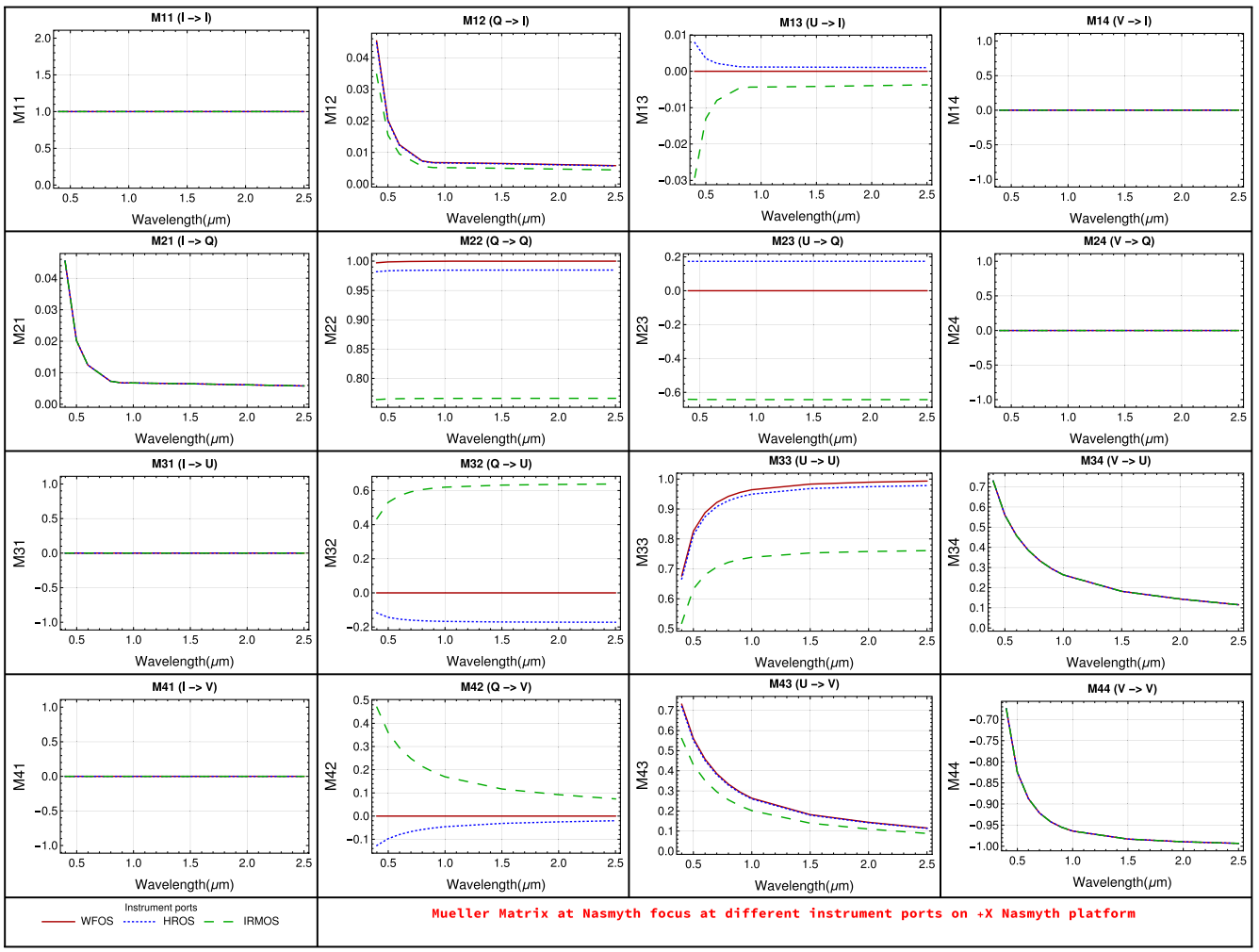

Fig. 14 Normalized Mueller matrix versus wavelength is estimated at different instrument ports on the $+X$ Nasmyth platform of TMT. WFOS is at IBA = IEA = 0, HROS is at IBA = 5, IEA = 0, and IRMOS is at IBA = −5.5, IEA = 0. These are indicated by different colors and line-styles.

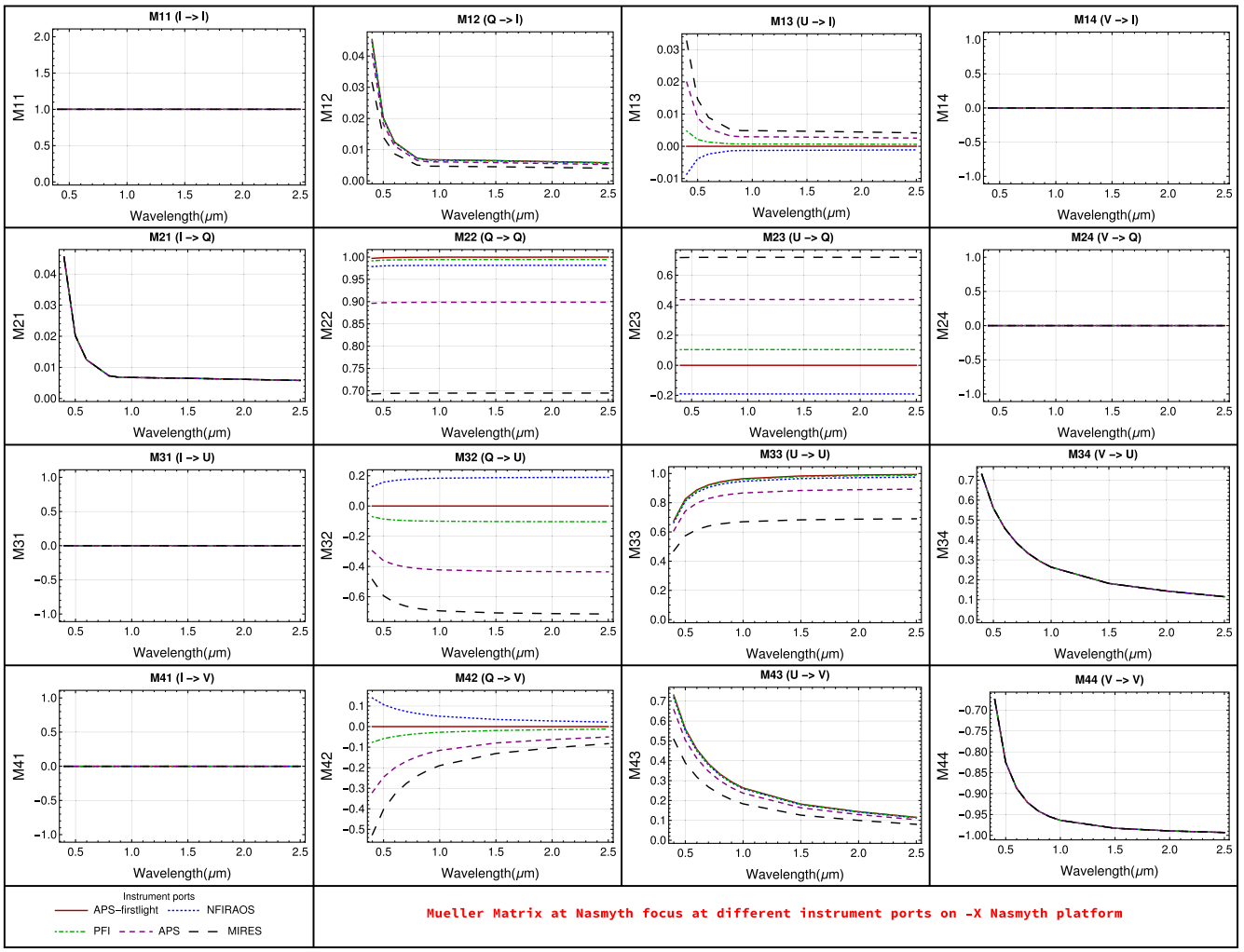

Fig. 15 Normalized Mueller matrix versus wavelength is estimated at different instrument ports on the $+X$ Nasmyth platform of TMT. APS first light is at IBA = 180, IEA = 0, NFIRAOS is at IBA = 174.5, IEA = 0, PFI is at IBA = 183, IEA = 0, APS is at IBA = 194, IEA = 0, and MIRES is at IBA = 203, IEA = 0. These are indicated by different colors and line-styles.

(WFOS port, IBA = 0) and M_{WFOS} is the Mueller matrix at the WFOS port ($\theta = 0$). These rotation matrices can be easily included in the data reduction pipeline for determining the polarization effects at different instrument ports.[31] The IP does not change with the rotation of the mirror as the tilt of the Nasmyth mirror remains the same at all the ports [see Eq. (3)]. Figures 14 and 15 show the variation in the Mueller matrix at different instrument ports on $+X$ and $-X$ Nasmyth platform, respectively.

For $\zeta \neq 0$, the θ and Φ vary at every instrument port except at WFOS port. The Mueller matrices are estimated at two instrument ports, one on $+X$ and the other on the $-X$ Nasmyth platform of TMT for varying zenith angles. The IP and CT are found to vary with the zenith angle of the telescope, as shown in Fig. 16. The variation in IP is 0.1% and in CT, it is 5% when the telescope is tracking an object from zenith angle 0 deg to 65 deg.

4.3 *Impact of Protected Silver Coating on Instrumental Polarization and Crosstalk*

The IP and CT values, as shown in Fig. 12, indicate that the polarization effects are comparatively higher in the blue region than the red region. Further analysis and estimation revealed that the high IP and CT values are due to the characteristics of silver, which are related to the complex refractive index of silver. The reflectivity plots for aluminum, bare silver, and protective silver can be found in Ref. 32, which show that silver has low reflectivity for the wavelength range of 0.3 to 0.45 μm. The real and imaginary parts of the refractive index of silver are almost equal. The Mueller matrix at the Nasmyth focus is obtained with bare aluminum coating for the comparison with the Gemini coating used in TMT and the results are reproduced in Fig. 17.

5 Impact on the Science Cases and Calibration Error

The polarimetric analysis of TMT carried out here computes the IP, CT, and DP across the field angles and the wavelengths that can be compared to the requirements of various observing programs. The calculated mean IP and CT values for the TMT Nasmyth focus must be considered as lower limits, since in a real scenario, the instrument would have additional effects due to variations in the coating and refractive indices, etc. The TMT PTRWG has collected about 35 science programs requiring polarimetric capability.[33] The suitability of TMT for all these science cases is available as a TMT internal document

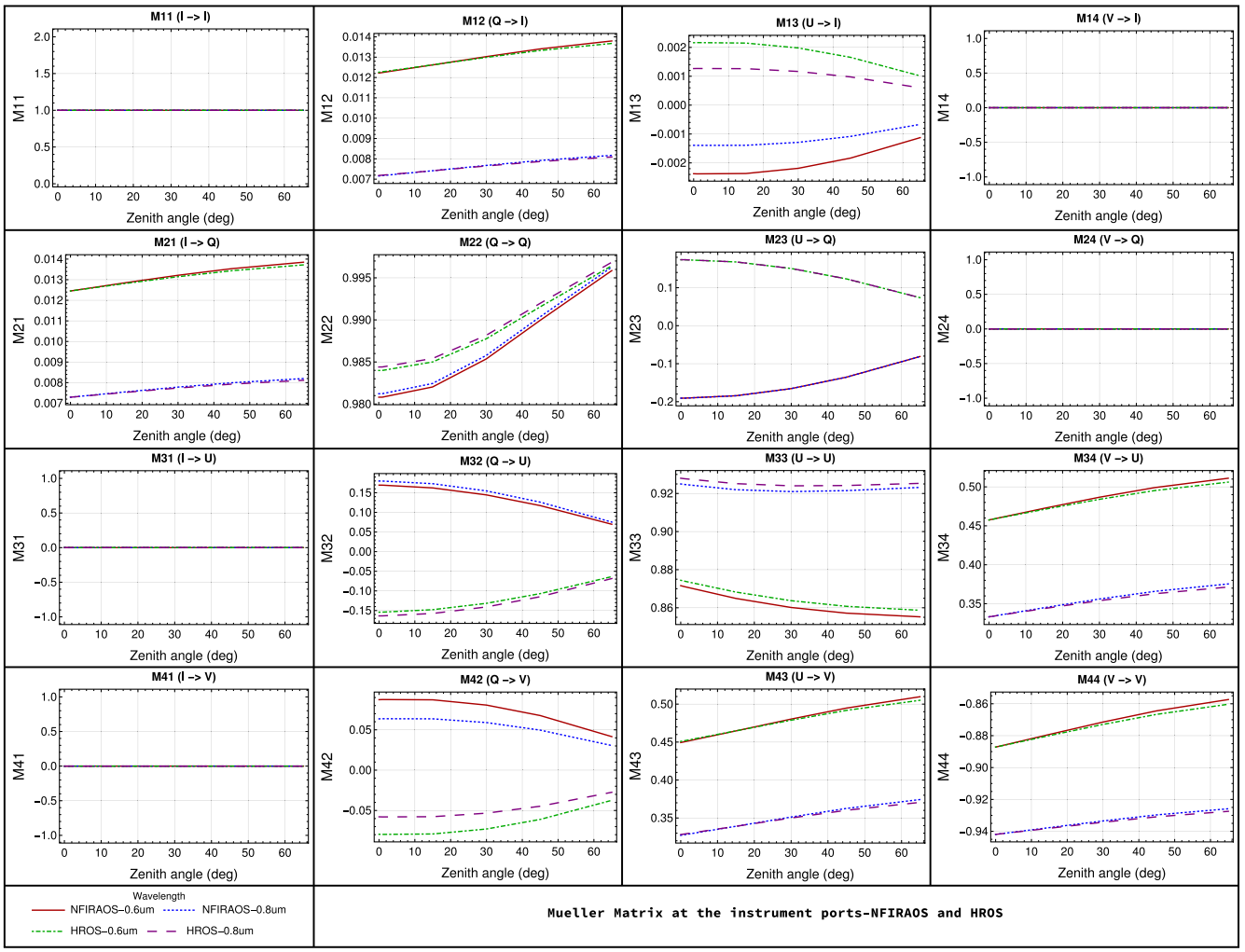

Fig. 16 Normalized Mueller matrix versus zenith angle is obtained at two different instrument ports on the Nasmyth platform of TMT. HROS is on the $+X$ and NFIRAOS is on the $-X$ Nasmyth platform. The colors and line-styles are used to indicate wavelength and instrument port.

(see TMT.PSC.TEC.14.007.DRF01).[34] We discuss here a few of those science cases as listed in Table 2. We have compared the requirements for each science program given in Table 2 against the values given in Table 1. The first three science programs can be attempted in the infrared wavelength regime and not in the optical wavelength regime (see Table 2) depending on their acceptable IP requirements. The first two programs do not have any specific requirements on the acceptable amount of CT and DP. The acceptable degree of CT is much lower than the estimated values for the third program. In the case of the observing program number 4, the IP and DP estimated are less than the requirements given. This can be completely supported by TMT with an appropriately designed instrument. The last two science programs in Table 2 with the requirement of acceptable IP on the order of 0.1% to 0.3% are unlikely to be supported. It is seen from Table 1 that in the mid- and far-infrared region, the IP, CT, and DP values are low, which allow us to consider the possibility of polarimetry in the Q and N bands.

5.1 *Mitigation and Calibration Strategies*

The polarization calibration error is dependent on systematic and measurement errors.[8] We note here that the IP calculated in the above analysis can be treated as a systematic error if all the mirror positions are properly controlled and calibrated. Thus, one should be able to calibrate and correct the data for the IP offset. The usual calibration method carried out in a Cassegrain telescope is recording the observations of standard polarized and unpolarized stars. This method of calibration can be carried out for this telescope, but this will obviously not reduce the actual level of IP. The ability to carry out science programs depends on the ability to determine an accurate calibration of the IP. The uncertainty of the calibration of the IP is typically a few % of the actual IP. Consequently, significantly reducing or mitigating the overall IP and therefore reducing the uncertainty on the calibration is an appealing strategy. One of the mitigation methods would be to use a compensating mirror[35,36] after the Nasmyth mirror before the polarimeter optics within the instrument. This mitigation technique has been implemented in SPHERE in VLT[37] and shows the residual IP of about 10^{-3}. The extent to which IP and CT due to TMT telescope optics can be nullified by this configuration has been worked out.[38] The compensating mirror $(M4)$ placed after the telescope focus gives an IP on the order of 10^{-5} and CT <1% for the field of view of 1 arc min in the entire wavelength region.[38]

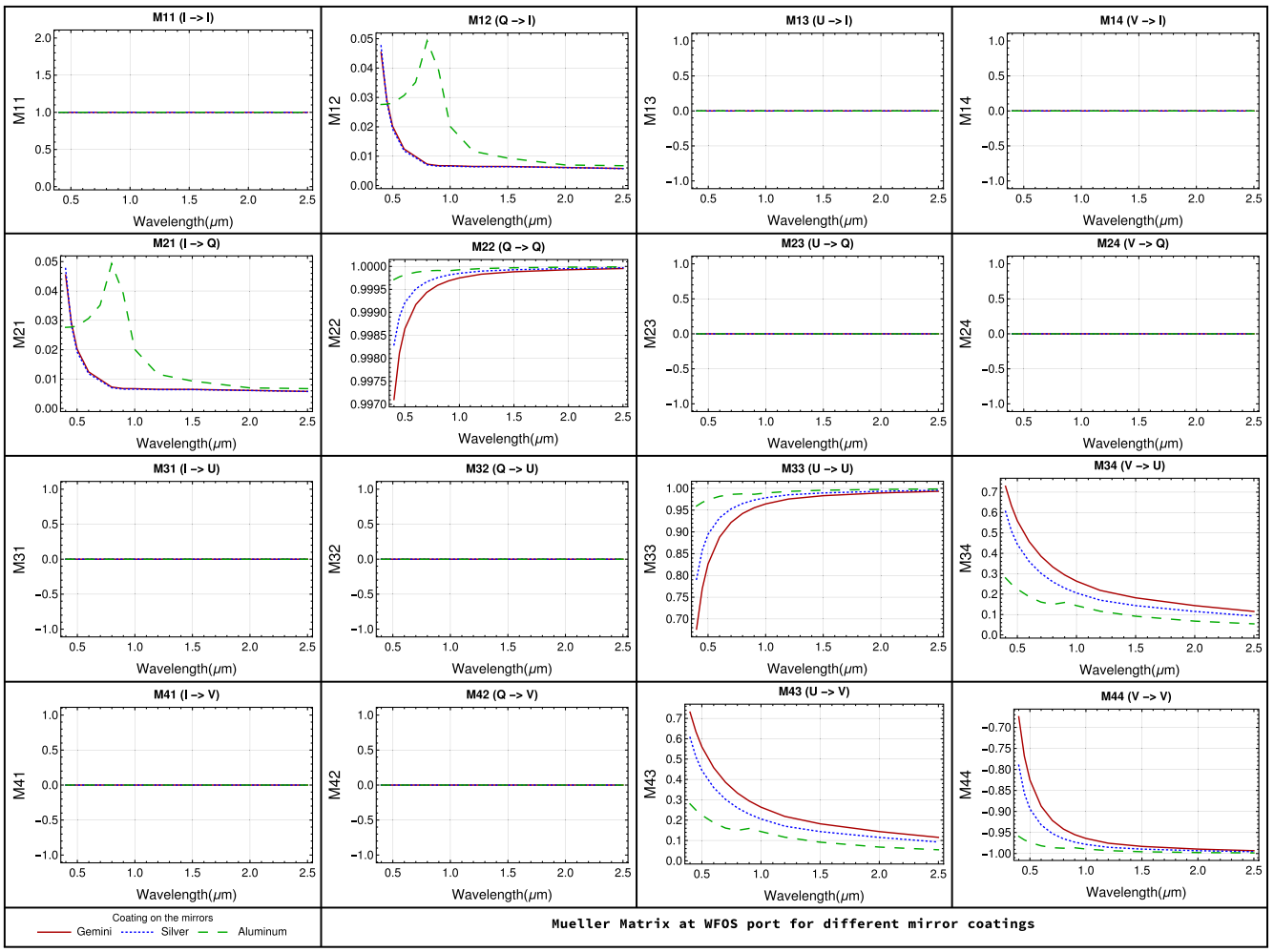

Fig. 17 The normalized Mueller matrix versus wavelength for different mirror coatings in TMT is obtained. Gemini, silver, and aluminum are indicated by different colors and line-styles.

6 Summary and Discussion

1. A detailed analysis of the polarization effects introduced by the optics of the TMT has been carried out. The analyses indicate that the Nasmyth mirror is the main source of the IP and CT at the focal plane, giving rise to an IP of 4.5% to 0.6%, CT of 73% to 11%, and DP of 2.2% to 0.5% in the wavelength range of 0.4 to 2.583 μm, respectively, for field angle and zenith angle equal to zero. These polarization effects vary with field angle and zenith angle of the telescope. The IP varies by 0.1% and CT by 5% when the zenith angle of the telescope varies from 0 deg to 65 deg. The IP and CT values are found to be asymmetric over the field-of-view of the telescope. The high values of CT in the optical region indicate that all the Stokes vectors have to be measured to reconstruct the input polarization.

2. The Mueller matrices are estimated and presented in Sec. 4 at all the instrument ports for different zenith angles, field angles, and wavelengths. These estimates would be critical in deciding the parameters for any future polarimetric instrument for TMT.

3. The impact of the polarization effects on the science programs has been assessed for a selection of example science programs that span the range of precision and sensitivity requirements. Science programs that require polarimetric measurements in the optical are unlikely to be supported with TMT, however, programs that require near-IR and mid-IR polarimetric measurements look to be achievable. Future work to study IP mitigation/reduction techniques is mentioned as this would undoubtedly facilitate more science programs by reducing the error on the IP calibration.

4. The calculated values are likely to be the lower limits. The measured IP, CT, and DP might be greater than the values we have estimated, since in our analysis, the coating of all the mirrors is considered to be ideal which might not be the case. Also, the $NiCrN_x$ layer may have an effect on the IP, CT, and DP estimates.

5. Since the primary mirror is considered to be monolith in our analysis, the impact of the gap and phasing of

Table 2 Science programs, observing requirements, and assessment results. The "acceptable IP" includes the contributions from the telescope and the instrument, including the adaptive optics system where appropriate.

Sl No.	Observing program and science cases	Wavelength region	Level of polarization per spatial and/or per spectral element	Field of view	Required S/N per wavelength bin	Limit of acceptable polarization calibration error	Acceptable instrumental polarization	Acceptable degree of CT	Acceptable amount of DP	Assessment
1	Chemical stratification and evaporation processes in comets	300–800 nm	0.4% to 15%	Extended nucleus slit length ~2 arc sec	~500	0.10%	~Few %	Not a significant problem	Not a significant problem	The estimated IP, CT, and DP values are within the acceptable limits only in the near IR region and not in the optical region.
2	Outflow geometry of quasars	Opt-NIR and 1 to 13 μm	0% to 40%	~5 arc sec	~10^3	0.1% to 1%	~1%	Not a significant problem	Not a significant problem	The estimated IP, CT, and DP values are within the acceptable limits only in near IR region and not in optical region.
3	Kinematic structure of CSM of young stars and brown dwarfs	370–1000 nm	~1%	Single object, seeing limited		0.10%	<1% req, <0.5% goal	~1%	~10%	The estimated IP, CT, and DP values are within the acceptable limits only in near IR region and not in the optical region.
4	High-contrast imaging of protoplanetary disk and magnetic field structure by polarized flux	1 to 2 μm J, H, K bands	5%	5 × 5 arc sec		0.10%	<2% req, <1% goal	Not a significant problem	<2%	The estimated IP, CT, and DP values are within the acceptable limits for the entire wavelength region. Can be supported by TMT.
5	Magnetic field of massive evolved stars, chemically peculiar stars and white dwarfs	350–1000 nm	0%–0.6% variable	Seeing limited point source	1000	0.01%	0.2% to 0.3%	Not a significant problem	Not a significant problem	The estimated IP, CT and DP values are beyond the acceptable limits for the entire wavelength region. Unlikely to be supported by TMT.
6	Vegetation red edge of exoplanets	600–800 nm	Upto 20% of planet flux	<3 arc sec	<10^4	0.01%	<0.1%	0.05%		The estimated IP, CT, and DP values are beyond the acceptable limits for the entire wavelength region. Unlikely to be supported by TMT.

the segments on the polarization has to be estimated. We are currently estimating the impact of these polarization effects on the point spread function of the telescope and nonpolarimetric performance of TMT. The results of this analysis will be presented in our next paper.

Appendix A: Polarization Ray Tracing Algorithm

A1 Primary Mirror

The primary mirror of the TMT is a concave hyperboloid,[30] which can be defined by the equation in the Cartesian coordinate system:

$$-\frac{x^2}{ap^2}-\frac{y^2}{ap^2}+\frac{(z+cp)^2}{cp^2}=1, \tag{4}$$

with the vertex of the hyperboloid at the origin. The values of ap and cp can be expressed in terms of the radius of curvature and the conic constant of the hyperboloid mirror. The incident ray can be represented by the DCs of the unit vector $\hat{i}$ as $(0, \sin\eta, -\cos\eta)$, where η is the field angle of the star with respect to telescope axis. The DCs of the normal to the mirror surface at every point (x, y, z) can be found, as described in Sen and Kakati.[23] The DCs of the reflected rays from the primary mirror surface can be represented by the unit vector:

$$\hat{r}=\hat{i}-2\hat{n}(\hat{i}\cdot\hat{n}), \tag{5}$$

where $\hat{n}$ is the unit vector in the direction normal at the point of incidence. The dot product between the DCs of the incident ray and the normal gives the incident angles for all the rays on the mirror surface. The Fresnel reflection coefficients are estimated,[29] as presented in Sec. 2.

Definition of 100% linearly polarized light: The electric field vector of the paraxial ray is considered to make an angle α with the y-axis (projection of celestial North–South) of the telescope. The DCs of this electric field vector are given as $(l_e, m_e, n_e) = (\sin\alpha, \cos\alpha, 0)$. Now, if the star is at a field angle of η with the optical axis of the telescope (Z-axis), then DCs of the electric field vector would change from the earlier situation where the field angle is zero. The electric field vector and the incident ray are orthogonal to each other. Using these conditions, we find the DC of the electric field vector, E_{dc} for the polarized light as $(\sin\alpha, \sin\alpha\cos\eta, -\sin\alpha\sin\eta)$.[23] The DCs of p and s vectors are represented as $\hat{s}_{incpri}=\hat{i}\times\hat{n}$, $\hat{p}_{incpri}=\hat{i}\times\hat{s}_{incpri}$, $\hat{p}_{refpri}=\hat{s}_{incpri}\times\hat{r}$. E_p. Further, E_s can be calculated from the relation:

$$E_p=E_{dc}\cdot\hat{p}_{incpri};\quad E_s=E_{dc}\cdot\hat{s}_{incpri}. \tag{6}$$

The amplitudes of the components of electric field vector of reflected ray in the p and s directions are related to the corresponding amplitudes of the incident ray by the following relations, where r_p and r_s are the reflection coefficients and E_p and E_S are the amplitudes of the electric field vector:

$$R_p=r_pE_p;\quad R_s=r_sE_s. \tag{7}$$

A2 Secondary Mirror

The secondary mirror of TMT is a convex hyperboloid, which is described by Eq. (8):

$$-\frac{x^2}{as^2}-\frac{y^2}{as^2}+\frac{(z-\tau)^2}{cs^2}=1, \tag{8}$$

where τ is the distance between the vertices of primary and secondary mirrors. The point of intersection on the secondary mirror for all the reflected rays reflected from the primary can be found. The DCs, incident angles, and reflection coefficients are determined for all the rays reflected from secondary (the details of the geometries can be followed from Ref. 23). The electric field of the light ray incident on the secondary mirror is the reflected electric field from the primary mirror having two components sE_p and sE_s given as follows:[23]

$$sE_p=(R_pD_{r1}+R_sD_{r2}), \tag{9}$$

$$sE_s=(R_pD_{r3}+R_sD_{r4}), \tag{10}$$

where

$$D_{r1}=\hat{p}_{refpri}\cdot\hat{p}_{inc\,sec};\quad D_{r2}=\hat{s}_{incpri}\cdot\hat{p}_{inc\,sec}, \tag{11}$$

$$D_{r3}=\hat{p}_{refpri}\cdot\hat{s}_{inc\,sec};\quad D_{r4}=\hat{s}_{incpri}\cdot\hat{s}_{inc\,sec}. \tag{12}$$

If the light originally incident on primary is unpolarized, then after reflection from the primary, we consider two components of it for our analysis at the secondary mirror surface: (1) polarized light (pp) and (2) unpolarized light (1-pp), where pp is the IP due to reflection from primary. Now, the polarized components will have their electric vectors in s and p directions (when reflected from secondary), given by

$$sR_p=sE_pr_{ps}pp;\quad sR_s=sE_sr_{ss}pp, \tag{13}$$

where r_{ps} and r_{ss} are the reflection coefficients for the secondary mirror. Similarly, for the unpolarized component, the electric vectors will be

$$sR_p=sE_pr_{ps}(1-pp);\quad sR_s=sE_sr_{ss}(1-pp). \tag{14}$$

A3 Nasmyth Mirror

Figure 1 shows various instrument configurations on the Nasmyth platform. The rotation and tilt of the mirror are dependent on the instrument position, instrument elevation, and the zenith angle of the telescope. The coordinate system used to derive these angles is explained in the TMT design requirements document:[30]

$$\theta=\arctan\left(\frac{\cos\zeta\cos(\mathrm{IEA})\sin(\mathrm{IBA})-\sin\zeta\sin(\mathrm{IEA})}{\cos(\mathrm{IEA})\sin(\mathrm{IBA})}\right), \tag{15}$$

$$\Phi=0.5\ \arccos[-\sin\zeta\cos(\mathrm{IEA})\sin(\mathrm{IBA})+\cos\zeta\sin(\mathrm{IBA})], \tag{16}$$

where ζ corresponds to the zenith angle of the telescope. It varies from 0 deg and 65 deg. IEA is the instrument elevation angle and IBA is the instrument bearing angle. θ and Φ

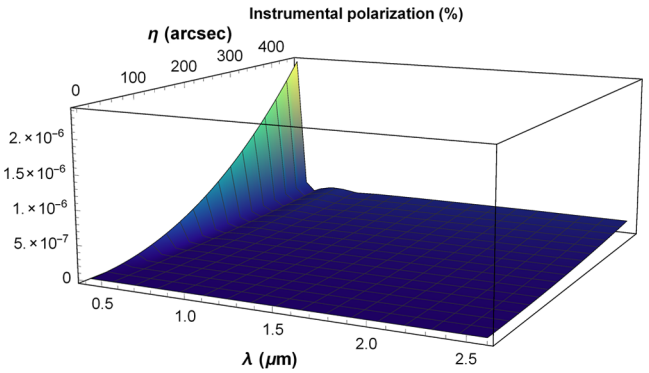

Fig. 18 Variation of IP for semifield of 7.5′ (z-axis) and the wavelength range of 0.4 to 2.5 μm (x-axis) is estimated at the prime focus. The blue region indicates low values of IP and yellow region indicates high values.

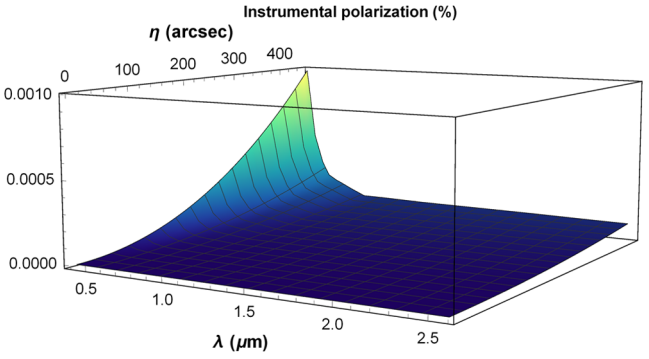

Fig. 19 Variation of IP for semifield of 7.5′ (z-axis) and the wavelength range of 0.4 to 2.5 μm (x-axis) is estimated at the Cassegrain focus of TMT. The blue region indicates low values of IP and yellow region indicates high values.

correspond to the rotation and the tilt of the Nasmyth mirror depending on the instrument position. The DC of the normal $(\hat{t}n)$ to the M3 mirror is given by (sin Φ cos θ, sin Φ sin θ, cos Φ). The incident angle, DC of the reflected ray, s-vector and p-vector directions are calculated using the previously discussed approaches. The electric fields of the light ray incident on the Nasmyth mirror (tE_p and tE_s) are estimated using Eq. (12) as it was done previously in the case of the secondary mirror. While considering unpolarized light incident on the primary and now reflected from the Nasmyth mirror surface, as before we consider two components of the light, one component (ss) fully polarized and another component $(1 - ss)$ unpolarized. The Stokes parameters in $p - s$ coordinate frame for the reflected electric field vector can be estimated[25] and are transformed into $X - Y$ coordinate system. Finally, these are integrated over the mirror surface.[23] The instrumental linear polarization (IP) is calculated at the Nasmyth focus for unpolarized light entering the telescope system, using the Stokes vectors given below. Again for 100% polarized light entering the telescope system, the DP and CT are calculated from the following relations:

$$\mathrm{IP} = \frac{\sqrt{Q^2 + U^2}}{I}, \tag{17}$$

$$\mathrm{DP} = \frac{I - (Q^2 + U^2 + V^2)}{I}; \quad \mathrm{CT} = \frac{V}{I}. \tag{18}$$

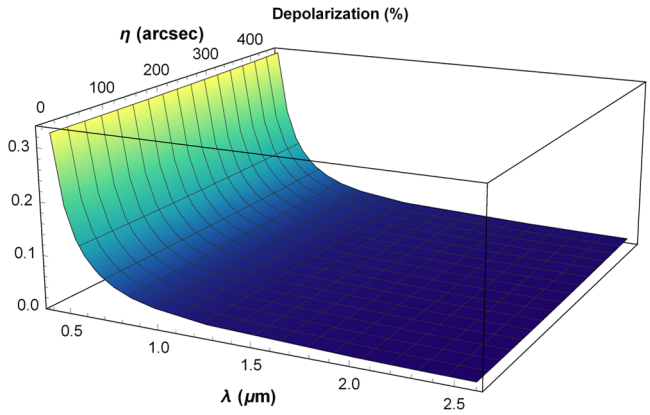

Fig. 20 Variation of DP for semifield of 7.5′ (z-axis) and the wavelength range of 0.4 to 2.5 μm (x-axis) is estimated at the prime focus. The blue region indicates low values of DP and yellow region indicates high values.

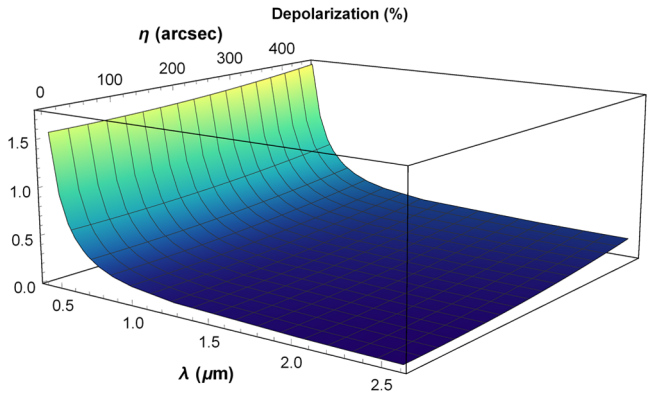

Fig. 21 Variation of DP for semifield of 7.5′ (z-axis) and the wavelength range of 0.4 to 2.5 μm (x-axis) is estimated at the Cassegrain focus of TMT. The blue region indicates low values of DP and yellow region indicates high values.

Acknowledgments

Authors would like to thank the referee for useful comments. Authors would also like to thank TMT project and all the members of the TMT polarimetry modeling team.

References

1. J.-L. Leroy, "Polarization of light and astronomical observation," *Adv. Astron. Astrophys.* **4** (2000).
2. J. P. McGuire, Jr. and R. A. Chipman, "Polarization aberrations in the SAMEX solar vector magnetograph," *Proc. SPIE* **0891**, 159–171 (1988).
3. J. Stenflo, "LEST update," in *High Spatial Resolution Solar Observations*, D. Neidig, Ed., p. 27, National Solar Observatory, Sunspot, New Mexico (1989).
4. S. Inoué and H. Kubota, "Diffraction anomaly in polarizing microscopes," *Nature* **182**(4651), 1725–1726 (1958).
5. J. B. Breckinridge, W. S. T. Lam, and R. A. Chipman, "Polarization aberrations in astronomical telescopes: the point spread function," *Publ. Astron. Soc. Pac.* **127**(951), 445–468 (2015).
6. J. Trujillo-Bueno, F. Moreno-Insertis, and F. Sánchez, *Astrophysical Spectropolarimetry*, Cambridge University Press, Cambridge (2002).
7. J. Sanchez Almeida and V. Martinez Pillet, "Instrumental polarization in the focal plane of telescopes," *Astron. Astrophys.* **260**, 543–555 (1992).

8. J. Tinbergen, *Astronomical Polarimetry*, Cambridge University Press, Cambridge (2005).
9. G. Van Harten, F. Snik, and C. Keller, "Polarization properties of real aluminum mirrors, I. Influence of the aluminum oxide layer," *Publ. Astron. Soc. Pac.* **121**(878), 377–383 (2009).
10. K. Sankarasubramanian, J. Samson, and P. Venkatakrishnan, "Measurement of instrumental polarisation of the Kodaikanal tunnel tower telescope," in *Solar Polarization*, K. N. Nagendra and J. O. Stenflo, Eds., pp. 313–320, Springer, Dordrecht (1999).
11. G. H. Sanders, "The Thirty Meter Telescope (TMT): an international observatory," *J. Astrophys. Astron.* **34**(2), 81–86 (2013).
12. R. Gilmozzi and J. Spyromilio, "The European extremely large telescope (E-ELT)," *Messenger* **127**, 11–19 (2007).
13. C. U. Keller, "Instrumentation for astrophysical spectropolarimetry," in *Astrophysical Spectropolarimetry*, Vol. **1**, pp. 303–354, Cambridge University Press, Cambridge (2002).
14. J. B. Breckinridge and B. R. Oppenheimer, "Polarization effects in reflecting coronagraphs for white-light applications in astronomy," *Astrophys. J.* **600**(2), 1091–1098 (2004).
15. G. Witzel et al., "The instrumental polarization of the Nasmyth focus polarimetric differential imager NAOS/CONICA (NACO) at the VLT—implications for time-resolved polarimetric measurements of Sagittarius A," *Astron. Astrophys.* **525**, A130 (2011).
16. M. de Juan Ovelar et al., "Instrumental polarisation at the Nasmyth focus of the E-ELT," *Astron. Astrophys.* **562**, A8 (2014).
17. J. Atwood et al., "Polarimetric analysis of the Thirty Meter Telescope (TMT) for modeling instrumental polarization characteristics," *Proc. SPIE* **9150**, 915013 (2014).
18. "The telescope optics," http://www.tmt.org/observatory/telescope/optics.
19. C. Baffes et al., "Primary mirror segmentation studies for the Thirty Meter Telescope," *Proc. SPIE* **7018**, 70180S (2008).
20. "TMT instruments," http://www.tmt.org/observatory/instruments.
21. R. M. Anche et al., "Analytical modelling of Thirty Meter Telescope optics polarization," *Proc. SPIE* **9654**, 965408 (2015).
22. R. A. Chipman, "Mechanics of polarization ray tracing," *Proc. SPIE* **1746**, 62–75 (1992).
23. A. Sen and M. Kakati, "Instrumental polarization caused by telescope optics during wide field imaging," *Astron. Astrophys. Suppl. Ser.* **126**(1), 113–119 (1997).
24. M. Born and E. Wolf, *Principle of Optics Electromagnetic Theory and Propagation, Interference and Diffraction of Light*, Pergamon Press, Oxford (1965).
25. E. Collett, *Polarized Light: Fundamentals and Applications*, Optical Engineering, Marcel Dekker Inc., New York (1992).
26. "Design requirement document for telescope optical coatings," TMT.OPT.DRD.09.003.DRF02, http://www.tmt.org/additional_documents/design-req-for-optical-coatings.pdf (18 September 2009).
27. T. Vucina et al., "Gemini's protected silver coatings: first two years in operation," *Proc. SPIE* **6273**, 62730W (2006).
28. E. D. Palik, *Handbook of Optical Constants of Solids*, Vol. **4**, Academic Press, Boston (1998).
29. H. A. Macleod, *Thin-Film Optical Filters*, CRC Press, Boca Raton, Florida (2001).
30. TMTGroup, "Design requirements document for tertiary mirror system M3S," TMT.OPT.DRD.07.006.REL29, http://www.tmt.org/sites/default/files/documents/application/pdf/design%20requirements%20document%202012-07.pdf (25July2012).
31. F. Joos et al., "Reduction of polarimetric data using Mueller calculus applied to Nasmyth instruments," *Proc. SPIE* **7016**, 70161I (2008).
32. "Silver vs Aluminum," http://www.gemini.edu/sciops/telescopes-and-sites/optics/silver-vs-aluminum.
33. "The polarimetric modelling results spread sheet," TMT.SEN.TEC.14.086.DRF01, https://docushare.tmt.org/docushare/dsweb/Get/Document-33026/tmtfinalresults_behaviors_20150818_master.xlsx (18 August 2015).
34. "Final Report on the Development of Polarimetric Performance Models and Assessment of Science Cases for TMT," TMT.PSC.TEC.15.007.REL01, https://docushare.tmt.org/docushare/dsweb/Get/Document-47249/polarization_modeling_results_final_version_TMTformat_20151029.docx (30 October 2015).
35. L. Cox, "The compensation of instrumental polarization by inclined mirrors," *Mon. Not. R. Astron. Soc.* **176**(3), 525–532 (1976).
36. J. Tinbergen, "Accurate optical polarimetry on the Nasmyth platform," *Publ. Astron. Soc. Pac.* **119**(862), 1371–1384 (2007).
37. R. Roelfsema et al., "The ZIMPOL high-contrast imaging polarimeter for SPHERE: polarimetric high-contrast commissioning results," *Proc. SPIE* **9909**, 990927 (2016).
38. R. M. Anche, G. C. Anupama, and K. Sankarasubramanian, "Preliminary design techniques to mitigate the polarization effects due to telescope optics of the Thirty Meter Telescope (TMT)," *J. Opt.* 1–8 (2017).

Ramya Manjunath Anche is a graduate student at the Indian Institute of Astrophysics. Currently, she is in the 6th year of the integrated Mtech-PhD program in astronomical instrumentation. For her PhD thesis, she is working on polarization capabilities in large telescopes.

Asoke Kumar Sen is a professor in the Department of Physics at Assam University, Silchar. He has been involved for more than twenty years in teaching optics, electromagnetism, relativity and astrophysics. His research interests are instrumentation for astronomical polarimetry and photopolarimetric observation of comets, star forming regions etc. He also works in laboratory bidirectional scattering experiment from regolith surface (analogue of asteroids' surface) and has a special interest in electromagnetism (optics) in curved space time.

Gadiyara Chakrapani Anupama is a professor at the Indian Institute of Astrophysics. Her expertise is in observational astronomy. Her primary research interest is in the area of time domain astronomy. Her other interests are in the development of astronomical facilities. She is involved with the TMT project as the Group Head of India-TMT Optics Group.

Kasiviswanathan Sankarasubramanian is division head of Space Science Division of Space Astronomy Group at ISRO Satellite Centre, Bengaluru, India. His area of expertise is polarimetry, solar magnetic field, optics, and solar instrumentation. Currently, he is PI for an x-ray spectrometer and also supporting the solar coronal polarimetric studies for an upcoming space mission. He is also involved in development of spectro-polarimetric instruments using novel techniques for ground based observatories.

Warren Skidmore is the Observatory Instrument System Scientist. He has been involved with the Thirty Meter Telescope Observatory Project since 2002 and has worked in site testing, supporting design teams, design tool validation, subsystem performance testing, development of the detailed science case, the science flow down to technical requirements and instrument development. His research interests are cataclysmic variables and accreting systems.